

# PCCP

Accepted Manuscript



This is an *Accepted Manuscript*, which has been through the Royal Society of Chemistry peer review process and has been accepted for publication.

*Accepted Manuscripts* are published online shortly after acceptance, before technical editing, formatting and proof reading. Using this free service, authors can make their results available to the community, in citable form, before we publish the edited article. We will replace this *Accepted Manuscript* with the edited and formatted *Advance Article* as soon as it is available.

You can find more information about *Accepted Manuscripts* in the [Information for Authors](#).

Please note that technical editing may introduce minor changes to the text and/or graphics, which may alter content. The journal's standard [Terms & Conditions](#) and the [Ethical guidelines](#) still apply. In no event shall the Royal Society of Chemistry be held responsible for any errors or omissions in this *Accepted Manuscript* or any consequences arising from the use of any information it contains.

**Exploring homo-FRET to quantify the oligomer stoichiometry of membrane-bound proteins involved in a cooperative partition equilibrium**

Ana M. Melo<sup>a</sup>, Aleksander Fedorov<sup>a</sup>, Manuel Prieto<sup>a</sup>, and Ana Coutinho<sup>\*a,b</sup>

<sup>a</sup> Centro de Química-Física Molecular and Institute of Nanoscience and Nanotechnology, Instituto Superior Técnico, Universidade de Lisboa, Av. Rovisco Pais, 1049-001 Lisboa, Portugal

<sup>b</sup> Dep. Química e Bioquímica, Faculdade de Ciências, Universidade de Lisboa, Campo Grande, 1749-016 Lisboa, Portugal

\* To whom correspondence should be addressed.

E-mail: [ana.coutinho@tecnico.ulisboa.pt](mailto:ana.coutinho@tecnico.ulisboa.pt)

## Abstract

The establishment of protein-protein interactions between membrane-bound proteins is associated to several biological functions and dysfunctions. Here, an analytical framework that uses energy homo transfer to directly probe quantitatively the oligomerization state of membrane-bound proteins engaged in a three-state cooperative partition is presented. Briefly, this model assumes that monomeric protein molecules partition into the bilayer surface and reversibly assemble into oligomers with  $k$  subunits. A general equation relating the overall steady-state fluorescence anisotropy of the sample to its fractional labeling was derived by considering explicitly that the anisotropy of mixed oligomers containing  $i$ -labeled monomers is inversely proportional to the number of labeled subunits per oligomer (Runnels and Scarlata limit). This method was very robust in describing the electrostatic interaction of Alexa 488 fluorescently-labeled lysozyme (Lz-A488) with phosphatidylserine-containing membranes. The pronounced decrease detected in the fluorescence anisotropy of Lz-A488 always correlated with the system reaching a high membrane surface density of the protein (at a low lipid-to-protein ( $L/P$ ) molar ratio). The occurrence of energy homo transfer-induced fluorescence depolarization was further confirmed by measuring the anisotropy decays of Lz-A488 under these conditions. A global analysis of the steady-state anisotropy data obtained under a wide range of experimental conditions (variable anionic lipid content of the liposomes,  $L/P$  molar ratios and protein fractional labeling) confirmed that membrane-bound Lz-A488 assembled into oligomeric complexes, possibly with a stoichiometry of  $k = 6 \pm 1$ . This study illustrates that even in the presence of a coupled partition/oligomerization equilibria, steady-state anisotropy measurements provide a simple and reliable tool to monitor the self-assembly of membrane-bound proteins.

## Introduction

The self-assembly of proteins on the membrane surface is involved in several biological functions and dysfunctions, which includes signal transduction<sup>1, 2</sup> and aggregation of amyloidogenic proteins/peptides,<sup>3, 4</sup> respectively. Therefore, the detection and determination of oligomerization states of membrane-bound proteins are of high relevance. Among the range of biophysical techniques available, the simple variant of Förster resonance energy transfer (FRET) that occurs between identical fluorophores, designated as homo-FRET, has emerged as an important tool to monitor protein oligomerization.<sup>5, 6</sup> As in hetero-FRET (when donor and acceptor are distinct fluorophores), the homo-FRET rate constant depends on the inverse sixth power of the distance between similar fluorophores on the nanometer scale (1-10 nm), and therefore, it is extremely sensitive to protein self-assembly for small cluster sizes.<sup>7</sup> Additionally, this technique simplifies the experimental procedure because it requires the use of a single fluorescent label. Since donors and acceptors have identical spectroscopic features, there is no donor quenching in a homo-FRET process. In fact, the extent of energy homo transfer can only be measured by quantifying its effect on the fluorescence depolarization (fluorescence anisotropy).<sup>8</sup> As demonstrated by Runnels and Scarlata,<sup>7</sup> when the inter fluorophore distances,  $R$ , within an oligomer are of the order of the Förster radius,  $R_0$ , the fluorescence anisotropy (either measurements of steady-state anisotropy,  $\langle r \rangle$ , or residual anisotropy,  $r_\infty$ ) is inversely proportional to the number of subunits in a oligomer. This situation corresponds to the limit of very efficient energy transfer between randomly oriented dipoles, when the depolarization due to rotational diffusion can be neglected.<sup>5-7</sup> Homo-FRET has been used extensively to study the aggregation of purified, labeled proteins/peptides.<sup>9-13</sup> Several of these studies aimed at retrieving structural information about the oligomers, for which time-resolved anisotropy measurements provide the most detailed information.<sup>10, 11</sup> More recently, the application of fluorescence anisotropy imaging microscopy has been expanding because it allows detecting and quantifying the molecular self-assembly of proteins and lipid clustering *in vivo*.<sup>5, 6, 14-18</sup>

In this study, we explored the potential of homo-FRET to determine the degree of oligomerization of membrane-bound proteins involved in a cooperative partition equilibrium.<sup>19-21</sup> Since Alexa Fluor 488 (A488) fluorescently-labeled lysozyme (Lz-A488) binding to phosphatidylserine-containing membranes has been shown earlier to

follow this three-state equilibria (membrane binding coupled to protein oligomerization)<sup>21, 22</sup>, it will be used here as a model system. Briefly, it was established that monomeric lysozyme molecules partitioned to the membrane surface and reversibly assembled into  $k$ -mers<sup>21</sup> (Fig. 1a). A global analysis of several membrane binding curves obtained for Lz-A488 under a wide range of experimental conditions concluded that the membrane-bound lysozyme oligomers contained  $k \geq 6$  subunits. Since A488 presents a small Stokes shift (Fig. 1b), a high quantum yield and a large extinction coefficient, we sought to further use this fluorescent tag in homo-FRET experiments to narrow down the stoichiometry of the membrane-bound lysozyme oligomers by measuring the fluorescence depolarization of Lz-A488 in the presence of anionic lipid membranes. Both steady-state and time-resolved fluorescence anisotropy measurements were performed for samples prepared with variable membrane surface concentrations of Lz-A488. Additionally, incomplete labeling (variable dye-to-protein molar ratios) induced changes in homo-FRET efficiency were also explored. The fluorescence anisotropy presented by each sample was described quantitatively by a general analytical model that took into account the contribution of all fluorescent species, namely free Lz-A488 molecules and both the membrane-bound monomeric and oligomeric species, and the occurrence of intra-subunit energy homo transfer within the lysozyme oligomers. A global analysis of the steady-state anisotropy data obtained according to this model was performed, allowing us to narrow down the oligomer stoichiometry of membrane-bound Lz-A488 to a minimum of  $k = 6 \pm 1$ . As exemplified in the present work, this model can be easily extended to other systems with coupled equilibria in which peptides or proteins bind to lipid membranes and concomitantly oligomerize on their surface, depending on their surface coverage of the vesicles.

## Experimental section

### Materials

1-Palmitoyl-2-oleoyl-*sn*-glycero-3-phosphocholine (POPC) and 1-palmitoyl-2-oleoyl-*sn*-glycero-3-phosphoserine (POPS) were obtained from Avanti Polar Lipids (Alabaster, AL). Lysozyme (EC 3.2.1.17) from chicken egg-white was purchased from Fluka Biochemika (Buchs, Switzerland). A488 succinimidyl ester (SE) (carboxylic acid, succinimidyl ester, mixed isomers, dilithium salt) and 4,4-difluoro-5,7-dimethyl-4-bora-3a,4a-diaza-*s*-indacene-3-propionic acid (BODIPY-FL) SE were obtained from Molecular Probes, Invitrogen (Eugene, OR). All organic solvents were of spectroscopic grade and were obtained from Merck (Darmstadt, Germany).

### Fluorescent labeling of lysozyme

Lysozyme was covalently labeled with A488 or BODIPY-FL SE dyes on its amine groups essentially as previously described.<sup>23</sup> Fluorescently-labeled lysozyme was separated from unreacted free fluorophore by gel filtration through a Sephadex G-25 gel filtration column equilibrated in 20 mM HEPES-KOH, 0.1 mM EDTA, pH 7.4 buffer. The degree of labeling (*DoL*) is the average number of labels covalently attached to lysozyme obtained during each conjugation procedure. This was calculated according to the standard UV-vis spectrophotometric method using the maximum extinction coefficient of the dyes,<sup>24</sup> and that of lysozyme in the UV,<sup>25</sup> to take into account the fluorophore's absorbance at 280 nm.<sup>24</sup> The fractional labeling, *f*, of each sample is the final ratio of dye molecules to protein molecules used in each assay (or experimental condition). Only in one set of measurements, the initial conjugation solution (with *DoL* = 0.54 (Table 1)) was further diluted with unlabeled protein and therefore its fractional labeling was lower than the initial degree of labeling of the sample, and dependent on the dilution factor used. Otherwise, the main procedure used in this work to vary the fractional labeling of each sample was to explore different labeling conditions (by varying the pH and/or dye-to-protein molar ratio used in the labelling reaction<sup>23</sup>). In this way, distinct Lz-A488 batches were prepared with variable degrees of labeling, *DoL*, which in all these cases were coincident with the final fractional labeling of the sample.

### Liposome preparation

POPC large unilamellar vesicles (LUVs) containing 20 or 30 mol% POPS were prepared by extrusion of lipid dispersions through 100-nm pore diameter polycarbonate membranes using 20 mM HEPES-KOH, 0.1 mM EDTA, pH 7.4 buffer as previously described.<sup>23</sup> The exact concentration of phospholipid stock solutions was determined using phosphate analysis.<sup>26</sup>

### Sample preparation

Each sample used for steady-state and time-resolved fluorescence measurements was prepared independently (*i.e.* no protein nor lipid titration were used) and incubated at least 1 h at room temperature prior to the measurements. In most of the experiments, the samples were prepared by changing its lipid-to-protein ( $L/P$ ) molar ratio using two different experimental approaches: (*i*) the phospholipid concentration was varied ( $0 < [L]_t < 6$  mM) while the protein concentration was kept fixed (0.5 or 3.0  $\mu$ M), or (*ii*) different protein concentrations (0 - 9  $\mu$ M) were added to the liposomes at 0.86 mM total phospholipid concentration. Additionally, different mixtures of labeled and unlabeled lysozyme were added to the liposomes to vary the fractional labeling of the sample in a wide range while keeping the total protein and lipid concentrations constant.

### Steady-state fluorescence anisotropy measurements

The steady-state fluorescence anisotropy measurements were performed on an SLM-AMINCO 8100 spectrofluorometer (SLM Instruments Inc., Urbana, IL) with double excitation and emission monochromators, fitted with automated rotating Glan-Thompson polarizers, and operating in “photon counting” mode. The steady-state anisotropy,  $\langle r \rangle$ , is defined as:<sup>27</sup>

$$\langle r \rangle = \frac{I_{VV} - G \cdot I_{VH}}{I_{VV} + 2 \cdot G \cdot I_{VH}} \quad (1)$$

where  $I_{VV}$  and  $I_{VH}$  are the fluorescence intensities (blank subtracted) of the vertically and horizontally polarized emission, when the sample is excited with vertically polarized light, respectively. The  $G$  factor ( $G = I_{HV}/I_{HH}$ ) is an instrumental correction factor, which takes into account the transmission efficiency of the monochromator to the polarization of the light. Samples were excited at 480 nm, and the polarized

emission was detected at 515 nm, both with a bandwidth of 4 nm. The effect of light scattering caused by the suspension of lipid vesicles<sup>28</sup> was taken into account by performing the same measurements with POPC liposomes as a control, since Lz-A488 does not partition significantly to neutral liposomes.<sup>23</sup>

Each Lz-A488 binding curve (steady-state anisotropy of Lz-A488 as a function of total phospholipid, protein concentration or fractional labeling of the sample) was measured once. Data is presented as average  $\pm$  standard deviation of 10 independent measurements of the steady-state anisotropy measured for each Lz-A488-containing sample. The quantitative analysis of the data was performed by globally analyzing seven binding curves obtained independently according to the three-state cooperative partition model derived in the manuscript.

### **Time-resolved fluorescence anisotropy measurements**

Time-resolved fluorescence anisotropy decays with picosecond resolution were obtained by the time-correlated single-photon timing technique essentially as previously described.<sup>29, 30</sup> The samples were excited at 460 nm by pulses from a frequency doubled, mode-locked Tsunami titanium:sapphire laser (Spectra Physics) pumped by a Nd:YVO<sub>4</sub> diode laser (model Millennia Xs from Spectra Physics). The parallel and perpendicular polarized components of the fluorescence ( $I_{VV}(t)$  and  $I_{VH}(t)$ , respectively) to the plane of polarization of the excitation beam were alternatively recorded. The fluorescence was detected by a Hamamatsu R-2809U microchannel plate photomultiplier at 515 nm that was selected using a Jobin-Yvon HR320 monochromator in combination with an adequate cut-off filter to avoid interference from Rayleigh-scattered light. The instrument response function (IRF) was recorded as excitation light scattered by a Ludox solution (silica, colloidal water solution, Aldrich, Milwaukee, WI). The data were collected in a multichannel analyzer with a time window of 1024 channels, at typically 15.3–16.8 ps/ channel, up to 50 000 and 20 000 counts in the peak channel of the IRF and decay curves, respectively.

The anisotropy decays obtained were globally analysed using the TRFA Data Processing Package version 1.4 of the Scientific Software Technologies Center (Belarusian State University) using a two-step procedure. First, the fluorescence decay

parameters were obtained by iterative convolution of the fluorescence decay,  $i_m(t)$ , with the IRF and fitting to the experimental data,  $I_m(t)$ , calculated as:

$$I_m(t) = I_{VV}(t) + 2 \cdot G \cdot I_{VH}(t) \quad (2)$$

using a nonlinear least-squares regression method.  $i_m(t)$  was fitted empirically to a sum of discrete exponential terms:

$$i_m(t) = \sum_{i=1}^n a_i \exp(-t/\tau_i) \quad (3)$$

where  $a_i$  and  $\tau_i$  are the amplitude and the lifetime of the  $i$ th decay component of fluorescence, respectively. In all cases, three decay times and a fourth, very short-lived, fixed component (compensating for any scattered excitation) gave the best fit to the fluorescence decays.<sup>21</sup> Then, the anisotropy decay parameters were obtained by simultaneous iterative convolution of  $i_{VV}(t)$  and  $i_{VH}(t)$ :

$$i_{VV}(t) = \frac{i_m(t)}{3} [1 + 2 r(t)] \quad (4)$$

$$i_{VH}(t) = \frac{i_m(t)}{3} [1 - r(t)] \quad (5)$$

with the IRF and globally fitting to the experimental parallel and perpendicular polarized components of the fluorescence intensity ( $I_{VV}(t)$  and  $I_{VH}(t)$ , respectively), after fixing in this analysis the fluorescence decay parameters to the values obtained after the first step. The fluorescence anisotropy decay curves,  $r(t)$ , were analyzed by a sum of discrete exponential terms:<sup>27</sup>

$$r(t) = \sum_{i=1}^n \beta_i \exp(-t/\phi_i) + r_\infty \quad (6)$$

where  $\beta_i$  and  $\phi_i$  are the normalized amplitude and the rotational correlation time of the  $i$ th decay component of anisotropy, respectively.  $r_\infty$  corresponds to the residual anisotropy, containing information about the restriction of the depolarizing process. The experimental steady-state fluorescence anisotropy,  $\langle r \rangle$ , was used as a constraint in the global analysis of the data, by introducing a  $G$  factor in this analysis that is related to the experimental data according to:

$$G = \frac{(1 - \langle r \rangle) \left( \int I_{VV}(t) dt \right)}{1 + 2\langle r \rangle \left( \int I_{VH}(t) dt \right)} \quad (7)$$

The instrumental  $G$  factor for our setup system is expected to be 1 because the polarized fluorescence light components were depolarized before the entrance slit of the monochromator. The  $G$  factor was introduced here only to account for experimental artifacts, namely, photobleaching of the fluorophore and laser fluctuations during the time-resolved fluorescence measurements.<sup>27</sup> As expected, this factor varied between 0.95 and 1.05. The goodness of the fits was evaluated by the reduced  $\chi^2$  value  $< 1.3$  and a random distribution of weighted residuals and autocorrelation plots. To further confirm the adequacy of the fit, the expected steady-state fluorescence anisotropy,  $\langle r \rangle_{ss}$ , was calculated using the parameters obtained from the time-resolved analyses:

$$\langle r \rangle_{ss} = \frac{\int_0^{\infty} i_m(t) \cdot r(t) dt}{\int_0^{\infty} i_m(t) dt} \quad (8)$$

and compared to the experimental steady-state fluorescence anisotropy measured for each sample (eqn (1)).

#### Determination of the Förster radius

Förster radius,  $R_0$ , or the critical distance at which the transfer efficiency is 50% for an isolated donor-acceptor pair, was calculated for the Lz-A488 molecules using the relationship:<sup>31</sup>

$$R_0 = 0.2108 \cdot [\kappa^2 \cdot \Phi_D \cdot n^{-4} \cdot J(\lambda)]^{1/6} \quad (9)$$

where the orientation factor,  $\kappa^2$ , and the refractive index of the medium,  $n$ , were assumed to be 2/3 (i.e. the dynamical isotropic limit value<sup>8</sup>) and 1.33, respectively. The donor quantum yield in the absence of acceptor,  $\Phi_D$ , for the monomeric free protein in buffer was determined to be 0.71 using a reference solution of fluorescein in 0.1 M NaOH ( $\Phi = 0.92$ <sup>32</sup>). The spectral overlap integral,  $J(\lambda)$  (in units  $M^{-1}cm^{-1}nm^4$ ) was calculated for Lz-A488 using its absorption and normalized fluorescence emission spectra in buffer solution.

## Theory

Homo-FRET has been shown previously to be a powerful tool to determine the oligomerization extent of both free and membrane-bound proteins on the nanometer scale.<sup>5-7, 9-13</sup> In fact, when energy homo transfer is a very efficient process among the fluorescently-labeled subunits included in a  $k$ -mer, it is possible to evaluate the oligomer stoichiometry in the system by observing its effect on the fluorescence anisotropy due to the strong depolarization of the fluorescence within each multimeric species.<sup>5-7</sup> Herein, we considered a more complex situation by including an extra protein/peptide partition equilibrium coupled to its reversible oligomerization on the membrane surface (cooperative partition). The distribution of monomeric protein/peptide between the aqueous ( $P_w^1$ ) and membrane ( $P_m^1$ ) phases is assumed to be governed by a partition coefficient,  $K_p$ . Upon reaching a critical surface concentration, the membrane-bound monomeric molecules self-associate into  $k$ -mers ( $P_m^k$ ) according to a discrete reversible oligomerization equilibrium described by a surface aggregation constant,  $K_{ag}$  (Fig. 1a).<sup>21</sup>

The additivity law of fluorescence anisotropy states that the steady-state fluorescence anisotropy,  $\langle r \rangle$ , of a sample can be described by a linear combination of the steady-state anisotropies characteristic of each species  $j$ ,  $\langle r \rangle_j$ , weighted by the respective molar absorption coefficient,  $\epsilon_j$ , molar fraction,  $x_j$ , and quantum yield,  $\Phi_j$ :<sup>8</sup>

$$\langle r \rangle = \sum_{j=1}^n \frac{\epsilon_j x_j \Phi_j}{\sum_{j=1}^n \epsilon_j x_j \Phi_j} \langle r \rangle_j \quad (10)$$

Considering that (i) the protein/peptide under study presents a fractional labeling  $f$ , (ii) the molar absorption coefficient of the fluorescently-labeled protein/peptide does not change upon its membrane binding and oligomerization, (iii) the aqueous and membrane-bound monomeric molecules display the same fluorescence quantum yield but the oligomeric species is quenched by a factor  $q = \Phi_{P_m^k} / \Phi_{P_m^1}$ , and finally (iv) energy homo transfer is exclusively an intra-oligomeric phenomenon, eqn (10) above reduces to the following for our three-state system:

$$\langle r \rangle = \frac{f x_{P_w^1}}{T} \cdot \langle r \rangle_{P_w^1} + \frac{f x_{P_m^1}}{T} \cdot \langle r \rangle_{P_m^1} + \frac{q x_{P_m^k}}{T} \cdot \langle r \rangle_{P_m^k} \quad (11)$$

Here,  $x_{p_w^1}$ ,  $x_{p_m^1}$  and  $x_{p_m^k}$  are the molar fractions of each species,  $\langle r \rangle_{p_w^1}$  and  $\langle r \rangle_{p_m^1}$  are the steady-state anisotropies of the monomer in aqueous solution and bound to the anionic lipid membranes, respectively, and  $T = f x_{p_w^1} + f x_{p_m^1} + q x_{p_m^k}$ . The anisotropy from the ensemble of mixed  $k$ -mers assembled in the membrane,  $\langle r \rangle_{p_m^k}$ , can be computed from the anisotropy of each oligomeric species containing  $i$  labeled subunits in the oligomer,  $\langle r \rangle_{p_m^k}^i$ , by further assuming that the occupancy level of the mixed oligomers, *i.e.* the fraction of  $i$  fluorescently labeled monomers per oligomer containing  $k$  subunits,  $P(i, f, k)$ , is described by the binomial distribution:<sup>33</sup>

$$P(i, f, k) = k! f^i (1 - f)^{(k-i)} / (i! (k - i)!) \quad (12)$$

Therefore,

$$\langle r \rangle_{p_m^k} = \sum_{i=1}^k \frac{i P(i, f, k)}{\sum_{i=1}^k i P(i, f, k)} \cdot \langle r \rangle_{p_m^k}^i \quad (13)$$

As previously shown by Runnels and Scarlata,<sup>7</sup> in the limit of a very efficiency energy transfer among randomly oriented fluorophores within an oligomer (interfluorophore distance  $R < 0.8 R_0$ ), the anisotropy of each oligomeric species,  $\langle r \rangle_{p_m^k}^i$ , is inversely proportional to the number  $i$  of labeled subunits in the oligomer if depolarizing rotation is absent:

$$\langle r \rangle_{p_m^k}^i = \langle r \rangle_{p_m^k}^{i=1} / i \quad (14)$$

where  $\langle r \rangle_{p_m^k}^{i=1}$  is the steady-state anisotropy of the oligomer containing only one labeled monomer (which cannot undergo homo-FRET). This value is anticipated to be much higher than the one presented by the membrane-bound monomeric molecules due to an increase in size/rigidity for these molecular assemblies. Under this limit, eqn (13) reduces to:

$$\langle r \rangle_{p_m^k} = \frac{[1 - (1 - f)^k]}{k \cdot f} \cdot \langle r \rangle_{p_m^k}^{i=1} \quad (15)$$

where  $(1 - f)^k = P(0, f, k) = 1 - \sum_{i=1}^k P(i, f, k)$  is the fraction of oligomers without labeled subunits. The homo-FRET ( $f, k$ ) term in this equation, *i.e.* the ratio  $\langle r \rangle_{p_m^k} /$

$\langle r \rangle_{P_m^k}^{i=1}$ , is plotted in Fig. 2 as a function of the fractional labeling for different oligomer stoichiometries. By taking into account that  $f$  is given by:

$$f = \frac{\sum_{i=1}^k iP(i, f, k)}{k} \quad (16)$$

it can be easily derived that  $\lim_{f \rightarrow 0}(\text{homo-FRET term}) = 1$  and  $\lim_{f \rightarrow 1}(\text{homo-FRET term}) = 1/k$ , as displayed in Fig. 2. This plot clearly shows that the larger the number  $i$  of fluorescently-labeled subunits in an oligomer, the lower the anisotropy of the overall fluorescence from the ensemble of mixed  $k$ -mers will be due to increasing contributions from homo-FRET. It also illustrates that homo-FRET measurements are more useful for tracking small oligomers since the incremental decrease in overall anisotropy becomes smaller as the degree of oligomerization increases.<sup>6</sup>

Finally, a simple analytical expression can be derived for the three-state system under study by combining eqn (11) and (15) above:

$$\langle r \rangle = \frac{x_{P_w^1}}{D} \cdot \langle r \rangle_{P_w^1} + \frac{x_{P_m^1}}{D} \cdot \langle r \rangle_{P_m^1} + \frac{[1 - (1 - f)^k] f^{-1} q x_{P_m^k}}{D} \cdot \langle r \rangle_{P_m^k}^{i=1} \quad (17)$$

with  $D = x_{P_w^1} + x_{P_m^1} + k q x_{P_m^k}$ . This equation clearly shows the contribution of each fluorescent species to the resulting overall steady-state anisotropy measured. Once the individual characteristic anisotropies of each fluorescent species ( $\langle r \rangle_{P_w^1}$ ,  $\langle r \rangle_{P_m^1}$  and  $\langle r \rangle_{P_m^k}^{i=1}$ , respectively) are obtained experimentally, eqn (17) can be fitted directly to the steady-state anisotropy data in order to discriminate the best oligomerization stoichiometry that describes the cooperative partition under study as previously described.<sup>21</sup>

## Results and discussion

### Rotational dynamics of fluorescently-labeled lysozyme in aqueous solution and bound to anionic lipid vesicles under the “infinite diluted regime”

The main goal of this work was to use homo-FRET measurements in order to evaluate the membrane-bound oligomer stoichiometry of fluorescently-labeled proteins/peptides engaged in a cooperative partition equilibria. The interaction of Lz-A488 with anionic lipid vesicles was recently described to follow such a three-state model<sup>21</sup> and therefore it will be used here as a model system. This conclusion was reached upon performing an extensive steady-state and time-resolved fluorescence characterization of the interaction of Lz-A488 with POPC LUVs containing 20 or 30 mol% POPS. Due to the strong electrostatic component of this interaction, the changes in the surface potential of the lipid vesicles upon binding of this highly cationic protein were taken explicitly into account in this work using the Gouy-Chapman theory.<sup>21</sup>

Lysozyme was covalently labeled with the succinimidyl ester of A488 on its amine groups.<sup>23</sup> Despite having seven amino groups (six  $\epsilon$ -amino groups of lysine and the *N*-terminal amine), several studies have shown that K33 and K97 are the best candidates for the modification sites in this protein because they are the most surface accessible and reactive lysine residues.<sup>34</sup> Additional experimental evidences obtained in our group<sup>21</sup> further suggest that K97 is most probably the major labeling site on this enzyme in agreement with the earlier suggestion made by Gorbenko and collaborators.<sup>35</sup> Since a low degree of labeling was always obtained ( $DoL = 0.21, 0.30, 0.50-0.54$ ), the majority of the protein molecules must be either unlabeled or singly-labeled with A488.<sup>23</sup> A careful photophysical characterization of each Lz-A488 batch was always performed. The fluorescence properties of Lz-A488 in buffer (fluorescence emission spectra, fluorescence emission decay kinetics<sup>21</sup> and steady-state and time-resolved fluorescence anisotropy) were found to be independent of both the degree of labeling and total protein concentration of the sample. Therefore, there was no evidence for spectroscopic heterogeneity between the distinct Lz-A488 batches used in this study.

As a first step, we set out to characterize the rotational dynamics of each monomeric species (aqueous and membrane-bound) present in our three-state system (Fig. 1). The steady-state fluorescence anisotropy measured for Lz-A488 in buffer solution (20 mM

HEPES-KOH, 0.1 mM EDTA, pH 7.4 buffer) was  $\langle r \rangle_{p^1} = 0.200 \pm 0.005$ . To gain a detailed description of the rotational depolarizing motions of the covalently-bound fluorophore that took place during its fluorescence time scale, time-resolved anisotropy decays were also measured, providing information about the amplitude of motion,  $\beta_i$ , and the time scale,  $\phi_i$ , on which this motion occurred. Two correlation times were required to describe the fluorescence anisotropy decays of Lz-A488 in buffer solution (Fig. 3) which are summarized in Table 1. Since the second rotational correlation time ( $\phi_2 = 5.2$  ns) was almost 20-fold longer than the shorter one ( $\phi_1 = 70$  ps), the total anisotropy can be interpreted as the product of two independent depolarizing processes. The fast correlation time is attributed to the rapid restricted movements resulting from local motions by the covalently linked probe and/or mobility of the protein segment to which it is attached,  $r_{\text{fast}}(t)$ , while the slow correlation time is related to the overall protein rotation in solution,  $r_{\text{slow}}(t)$ :<sup>36, 37</sup>

$$r(t) = r_{\text{slow}}(t) \cdot r_{\text{fast}}(t) \quad (18)$$

where

$$r_{\text{slow}}(t) = \exp(-t/\phi_{\text{global}}) \quad (19)$$

and

$$r_{\text{fast}}(t) = r(0) \left[ (1 - S_{\text{seg}}^2) \cdot \exp(-t/\phi_{\text{seg}}) + S_{\text{seg}}^2 \right] \quad (20)$$

Here,  $S_{\text{seg}}$  is the order parameter characterizing the restricted range of internal angular fluctuations of the protein segment containing the covalently-bound dye ( $S_{\text{seg}}^2 = \beta_2/(\beta_1 + \beta_2)$ ). The short and long rotational correlation times obtained from the fit (Table 1) are respectively related to  $\phi_{\text{seg}}$  and  $\phi_{\text{global}}$  by

$$\phi_1 = \left( \frac{1}{\phi_{\text{seg}}} + \frac{1}{\phi_{\text{global}}} \right)^{-1} \quad (21)$$

$$\phi_2 = \phi_{\text{global}} \quad (22)$$

**Table 1** – Time-resolved fluorescence anisotropy parameters (rotational correlation times,  $\phi_i$ , normalized amplitudes,  $\beta_i$ , and residual anisotropy,  $r_\infty$ ) of Lz-A488 in aqueous solution and in the presence of POPC:POPS 80:20 LUVs (at different  $L/P$  molar ratios) obtained from fitting eqn (6) to the anisotropy decays presented in Figs. 3 and 5. The experimental steady-state fluorescence anisotropy,  $\langle r \rangle_{\text{exp}}$ , and the one calculated from the parameters obtained from the time-resolved analyses,  $\langle r \rangle_{\text{ss}}$  (eqn (8)) are also presented.

$[L]_t$ (mM)	$[Lz]_t$ ( $\mu\text{M}$ )	$f$	$\beta_1$	$\phi_1$ (ns)	$\beta_2$	$\phi_2$ (ns)	$r_\infty$	$\chi_G^2$	$\langle r \rangle_{\text{exp}}$	$\langle r \rangle_{\text{ss}}$
0	1.5	0.21	0.07	0.07	0.32	5.2	-	1.29	0.200 $\pm 0.005$	0.195
0.86	0.3	0.54	0.04	0.34	0.25	7.3	0.05	1.11	0.229 $\pm 0.009$	0.227
0.86	6.0	0.03	0.05	0.07	0.11	5.2	0.22	1.01	0.286 $\pm 0.017$	0.285
0.86	6.0	0.11	0.06	0.17	0.14	4.6	0.16	1.10	0.247 $\pm 0.003$	0.246
0.86	6.0	0.23	0.07	0.22	0.13	3.4	0.12	1.03	0.198 $\pm 0.006$	0.197
0.86	6.0	0.34	0.10	0.19	0.13	3.2	0.09	1.01	0.169 $\pm 0.007$	0.167
0.86	6.0	0.54	0.09	0.43	0.11	6.1	0.04	1.24	0.142 $\pm 0.007$	0.140
4.0	0.5	0.21	0.07	0.14	0.19	6.4	0.11	1.12	0.244 $\pm 0.013$	0.241

The recovered value for  $\phi_{\text{global}} = 5.2$  ns is in good agreement with the theoretical prediction from the Perrin equation for the overall rotation in aqueous solution of a rigid hydrated sphere ( $\phi = 5.5$  ns for the native lysozyme ( $M_r = 14.3$  kDa) in aqueous solution at 23 °C, and assuming 20% hydration and a partial specific volume of 0.74 cm<sup>3</sup>/g)<sup>27</sup>, confirming the assignment of the slow motion of Lz-A488 to the whole rotation of the protein. The segmental correlation time ( $\phi_{\text{seg}} = 68$  ps) reflects an average of the fast localized motions of the covalently-bound fluorescent dye. Since these are restricted, and consequently the randomization of orientations is not achieved, the anisotropy at

long times should not decay to zero. However, the overall rotation of the protein is responsible for the decay of its fluorescence anisotropy to zero. The range of angular displacement of these motions can be derived from  $S_{\text{seg}}$  assuming a “wobbling-in-cone” model,<sup>38</sup> in which the transition dipole moment of the dye is assumed to move freely within a cone with a fixed half-angle. In this framework, the half-angle,  $\theta_{\text{seg}}$ , of the cone within which the segment containing the covalently-attached dye freely rotates is given by,

$$\cos \theta_{\text{seg}} = \frac{1}{2} \left[ (8 S_{\text{seg}} + 1)^{1/2} - 1 \right] \quad (23)$$

An angle of  $\theta_{\text{seg}} = 20^\circ$  was obtained for LZ-A88 in buffer, implying that this segment experiences relatively small angular displacements with respect to the protein as a whole during the A488 excited state lifetime. The constraints on the local motions of the dye are due to the short covalent linkage between the dye and the protein and steric hindrances caused by the protein surface,<sup>27</sup> as well as to the probable electrostatic interactions between the negatively charged dye and lysozyme.<sup>39</sup> Finally, the time-zero anisotropy ( $r(0) = \beta_1 + \beta_2 = 0.39$  (Table 1)) was similar to the one measured for A488 in a rigid environment, ( $r_0 = 0.376$ ).<sup>40</sup>

To confirm that the main factor responsible for the rather high steady-state anisotropy value measured for LZ-A488 in aqueous solution was the limited range of local/segmental motions presented by the covalently-bound A488 probe, lysozyme was also derivatized with BODIPY-FL, a neutral fluorophore with a slightly longer covalent linker.<sup>24</sup> The steady-state fluorescence anisotropy of LZ-BODIPY in aqueous solution was lower than the value measured under the same conditions for LZ-A488 ( $\langle r \rangle = 0.073 \pm 0.070$ ). This result can be partially explained by the longer intensity-weighted mean lifetime of LZ-BODIPY as compared to LZ-A488 ( $\langle \tau \rangle_1 = 5.5$  ns *versus* 3.4 ns). The time-resolved anisotropy decay of LZ-BODIPY in aqueous solution was also described by two correlation times ( $\phi_1 = 0.33$  ns and  $\phi_2 = 3.8$  ns) with similar amplitudes ( $\beta_1 = 0.14$  and  $\beta_2 = 0.13$ ) (Fig. S1). In this case, the apparent time-zero anisotropy ( $r(0) = \beta_1 + \beta_2 = 0.27$ ) was significantly lower than the fundamental anisotropy reported for the free dye ( $r_0 = 0.370$ ),<sup>41</sup> indicating that there are ultrafast motions of the covalently-bound dye relatively to the native protein which cannot be observed within the time resolution of our instrumental step-up. In addition, the half-angle associated to the

“wobbling” motion of BODIPY covalently-tagged to the protein was higher ( $\theta_{\text{seg}} = 38^\circ$ ) than the one obtained for Lz-A488, confirming our previous reasoning. Note that due to the lower amplitude associated to the whole rotation of the protein, it was difficult to recover its correlation time, which was lower than the one obtained for Lz-A488 or the theoretically expected value.

We next sought to obtain information about the rotational properties of the monomeric membrane-bound Lz-A488. As shown before,<sup>21</sup> the experimental conditions that maximize the molar fraction of this species in our system involve preparing samples using a high  $L/P$  molar ratio to attain the so-called “infinite diluted regime” on the membrane surface. The steady-state anisotropy of 0.5  $\mu\text{M}$  Lz-A488 ( $f = 0.54$ ) was found to increase essentially monotonically from  $\langle r \rangle = 0.198 \pm 0.007$  measured for the free protein to  $\langle r \rangle = 0.247 \pm 0.005$  as the total lipid concentration (POPC:POPS 80:20 LUVs) in solution increased from 0.1 to 6 mM (Fig. 4a). For this particular experimental condition, the variation of the steady-state anisotropy of Lz-A488 with the total lipid concentration mainly reflects lysozyme partition to the anionic lipid vesicles, and  $\langle r \rangle_{\text{p}_m} = 0.25$  can be estimated from this data. Noteworthy, as it is exemplified in Fig. 3 for 0.5  $\mu\text{M}$  Lz-A488 ( $f = 0.21$ ) in interaction with 4 mM POPC:POPS 80:20 LUVs, the fluorescence anisotropy decay of membrane-bound monomeric Lz-A488 under this regime is more complex than the one obtained in aqueous solution because it presents now a residual component at long times ( $r_\infty = 0.11$  (Table 1)). This can be readily explained by the hindered rotational diffusion of membrane-bound Lz-A488 that does not allow a complete randomization of the fluorophore orientation during its excited-state lifetime. The parameters obtained from the fit are summarized in Table 1. As expected, a slower correlation time ( $\phi_2 = 6.4$  ns) than the one obtained for the free protein was also recovered.

### **Evidences for energy homo transfer in the mixed oligomers from steady-state and time-resolved anisotropy measurements**

The extent of homo-FRET is expected to be critically dependent on the membrane surface density of Lz-A488 attained in our three-state system. When the samples are prepared with a low  $L/P$  molar ratio, the oligomerization equilibrium should be shifted toward the membrane-bound oligomeric pool in dynamic equilibrium with the

monomer.<sup>21</sup> As the probability for energy homo transfer among the fluorescently-labeled subunits incorporated in each mixed oligomers is enhanced in these samples, this should lead to an overall decrease of their steady-state fluorescence anisotropy. In fact, the hallmark of homo-FRET is that the lifetime is unaffected but, unless the two transition dipoles are parallel, additional depolarization occurs. Certainly, energy migration among the Lz-A488 molecules must be an efficient process since a relatively large Förster radius,  $R_0 = 4.8$  nm, was calculated for the membrane-bound monomeric Lz-A488 at the “infinite dilution regime” (*i.e.* using a very high  $L/P$  ratio). When the previously reported quenching of Lz-A488 upon its oligomerization in the membrane<sup>21</sup> is taken into account,  $R_0$  reduces only to 4.2 nm. This Förster radius compares well with the dimensions of lysozyme (a prolate ellipsoid of  $3.0 \times 4.5$  nm)<sup>42</sup> and is large enough to make energy transfer between the subunits an efficient process, particularly for small oligomers present on the membrane surface.

Two experimental approaches were used here to maximize the molar fraction of the membrane-bound oligomeric species:<sup>21</sup> (*i*) the fixed protein concentration used in the assays was increased to 3.0  $\mu\text{M}$  while the total phospholipid concentration was again varied between  $0 < [L]_t < 6$  mM (Fig. 4b), or (*ii*) increasing lysozyme concentrations (0 - 9  $\mu\text{M}$ ) were added to the liposomes at a fixed 0.86 mM total phospholipid concentration (Fig. 4c). When the protein concentration was augmented 6-fold (from 0.5  $\mu\text{M}$  to 3  $\mu\text{M}$ ,  $f = 0.54$ ), the steady-state anisotropy no longer presented a hyperbolically dependency with the total lipid concentration used in the assay. At first, it sharply decreased from  $\langle r \rangle = 0.212 \pm 0.004$  to  $0.154 \pm 0.009$  as the lipid concentration increased up to 0.3 mM POPC:POPS 80:20 LUVs. This tendency was then reverted as this parameter progressively increased towards  $\langle r \rangle = 0.230 \pm 0.003$  at 6 mM total lipid concentration (Fig. 4b). As expected, and according to our previous study,<sup>21</sup> the pronounced decrease of the steady-state anisotropy at a low  $L/P$  ratio is highly correlated with the extent of lysozyme oligomerization on the membrane surface and can therefore be ascribed to an efficient intraoligomeric homo-FRET. This was further confirmed when the second experimental approach was used since the steady-state anisotropy was found to monotonically decrease as the total lysozyme concentration added to the liposomes at 0.86 mM (POPC:POPS 80:20 LUVs) varied from 0 to 9  $\mu\text{M}$  ( $f = 0.54$ ) (Fig. 4c). It should be stressed that these results cannot be explained by the previously reported concomitant decrease of the mean fluorescence lifetime of Lz-A488

at low  $L/P$  molar ratios<sup>21</sup> because this would lead to an increase of Lz-A488 fluorescence anisotropy, as predicted by the Perrin equation.<sup>27</sup> In addition, in the absence of energy homo transfer, the self-assembly of the A488 covalently-labeled enzyme molecules into oligomers is expected to produce an increase of their steady-state fluorescence anisotropy due to their increased size/molecular packing (see below), at variance with the reported changes. Interestingly, when the labeling stoichiometry of the samples used in the first experimental approach was reduced by half ( $f= 0.30$  instead of  $f= 0.54$ ) while the total protein concentration of the samples was kept constant at 3  $\mu\text{M}$ , the biphasic behavior of the steady-state anisotropy was not as dramatic as before (Fig. 4b), reaching a minimal  $\langle r \rangle = 0.185 \pm 0.007$  at 0.6 mM total lipid concentration. Since the molar fraction of each fluorescent species in these two experimental situations are invariant as they are governed by the total protein and phospholipid concentrations present in each sample,<sup>21</sup> this result can only be explained by a lower level of occupancy of the mixed oligomers assembled at the membrane surface, which produces a decrease in their intraoligomeric energy homo transfer efficiency.

The steady-state data presented so far strongly support the occurrence of an efficient intra-oligomeric energy homo transfer at high membrane surface densities of Lz-A488. This conclusion was further confirmed by performing time-resolved fluorescence anisotropy measurements for some of the samples. As exemplified in Fig. 5a, upon increasing the lysozyme concentration added to 0.86 mM POPC:POPS 80:20 LUVs from 0.3 to 6.0  $\mu\text{M}$  ( $f= 0.54$ ), a much faster decay component was detected in the time-resolved anisotropy decay, which also presented a lower apparent time-zero anisotropy ( $r(0)= 0.24$  instead of 0.34 (Table 1)). Both these alterations reflect that under this experimental condition the system displays an ultrafast homo-FRET component contributing to the fluorescence depolarization of Lz-A488<sup>43</sup> that cannot be totally resolved by our instrumental step-up.

According to eqn (17), two conditions should be met to allow for a reliable determination of the steady-state anisotropy of the oligomers not affected by a energy homo transfer process,  $\langle r \rangle_{\text{pk}}^{i=1}$  (*i.e.* the steady-state anisotropy of mixed oligomers containing only one labeled monomer). First, the oligomerization equilibrium should be strongly displaced towards the assembly of membrane-bound  $k$ -mers. Secondly, the

fractional labeling of the sample should be as low as possible (Fig. 2), provided the fluorescence measurements still display a good signal-to-noise ratio. Therefore, several samples were prepared at the same low  $L/P$  ratio (6  $\mu\text{M}$  lysozyme was added to 0.86 mM POPC:POPS 80:20 LUVs) but using variable mixing ratios of fluorescently-labeled and unlabeled protein (*i.e.* with a variable  $f$ ) (Fig. 4d). As expected, an increase in the steady-state anisotropy was observed as the fractional labeling of the sample decreased, reflecting the statistically reduction of the occupancy level of the oligomer with labeled monomers. More importantly, when only *ca.* 3% of the lysozyme molecules bore a covalently-tagged A488 fluorophore, the steady-state anisotropy reached  $\langle r \rangle = 0.29 \pm 0.02$ , slightly higher than  $\langle r \rangle_{\text{p}_m^1} = 0.25$ , confirming that the larger size/greater rigidity of the membrane-bound oligomers produces a decrease in the rotational mobility of their Lz-A488 subunits. The concomitant changes produced in the fluorescence anisotropy decays of these samples were even more dramatic, as it is shown in Fig. 5b. The anisotropy decays, which were again analyzed considering two rotational correlation times plus a residual component at long times,  $r_\infty$ , displayed a significant and very sharp increase of  $r_\infty$  from 0.04 to 0.22 when the fractional labeling of the sample decreased from  $f = 0.54$  to  $f = 0.03$  (Table 1). This result is the experimental signature for energy homo transfer.<sup>43</sup> It should also be kept in mind that due to the coupled nature of the two equilibria considered here, there is always a significant fraction of aqueous monomeric fluorescently-labeled protein contributing to a fast depolarization of the sample fluorescence at short times.

According to the arguments discussed above, the lysozyme sample prepared with a very low fractional labeling ( $f = 0.03$ ) is particularly important in our work because it can be used to retrieve  $\langle r \rangle_{\text{p}_m^k}^{i=1}$ , as it is illustrated in Fig. 2. For each previously optimized pair  $k$  (integer) and  $K_{\text{ag}}$  describing the oligomerization of Lz-A488 in the membrane, we calculated the molar fractions of each species present in the system using the methodology implemented earlier (see below).<sup>21</sup> These values, together with the experimental steady-state anisotropy of this particular sample, were then used to solve eqn (17) in order to get  $\langle r \rangle_{\text{p}_m^k}^{i=1}$ . We obtained  $\langle r \rangle_{\text{p}_m^k}^{i=1} = 0.352 \pm 0.07$  for  $2 < k < 10$  and therefore this value was held fixed in the subsequent analyses. This result confirms the reduced rotational dynamics displayed by the Lz-A488 subunits upon their assembly into oligomers.

### Determination of the oligomer stoichiometry of membrane-bound proteins involved in a cooperative partition equilibrium using energy homo transfer measurements

Finally, to estimate the membrane-bound oligomer stoichiometry, a global fitting of eqn (17) to the experimental data of  $\langle r \rangle$  vs [Phospholipid]<sub>t</sub>,  $\langle r \rangle$  vs [Lysozyme]<sub>t</sub> and  $\langle r \rangle$  vs fractional labeling,  $f$ , was performed. The data obtained in seven independent experiments employing different experimental conditions, namely, two different mol% of POPS (20 and 30 mol%) and three orthogonal experimental designs (Fig. 4a-d and S2) were used in this fitting. For each experimental condition (total lipid concentration of liposomes prepared with a specific anionic lipid content and lysozyme concentration with a fractional labeling ratio,  $f$ ), a set of pre-optimized pairs of  $k$  (integer) and  $K_{ag}$  values was used to solve the mass action law of the coupled equilibria as previously described.<sup>21</sup> The solution obtained for each case was then used to calculate the molar fractions of aqueous and membrane-bound monomeric lysozyme ( $x_{p_w^1}$  and  $x_{p_m^1}$ , respectively) and oligomeric lysozyme ( $x_{p_m^k}$ ).<sup>21</sup> As described above, a careful photophysical characterization of this three-state system allowed to hold  $q = 0.5$ <sup>21</sup>  $\langle r \rangle_{p_w^1} = 0.205$ ,  $\langle r \rangle_{p_m^1} = 0.250$  and  $\langle r \rangle_{p_m^{i=1}} = 0.350$  fixed in these analyses. This is important due to the strong correlation between several of the parameters present in our model. The mean-square deviation (MSD) function:

$$\text{MSD} = \sum_{i=1}^n (\langle r \rangle_{\text{exp}} - \langle r \rangle_{\text{calc}})^2 / \nu \quad (24)$$

was then calculated, where  $n$  and  $\nu$  are the number of experimental points (with  $n = 75$ ) and degrees of freedom in the fitting procedure, respectively. From Fig. 6, it can be concluded that the oligomerization stoichiometry of membrane-bound lysozyme is centered around  $k = 6 \pm 1$ . An excellent fit of our homo-FRET model to the experimental data of steady-state fluorescence anisotropy was obtained, as it is illustrated in each panel of Fig. 4 and S2 for  $k = 6$  and  $K_{ag} = 2 \times 10^{14}$ . The individual contributions of each fluorescent species present in this three-state system to the resulting overall steady-state anisotropy (eqn (17)) are also plotted in these panels to allow for a better appreciation of the complexity of the coupled equilibria under study. In this regard, it should be noted that reducing the fractional labeling of the sample

increases the anisotropy from the mixed oligomers but leaves the anisotropy of the monomers unchanged, as expected (Fig. 4b and d).

### Revisiting the model assumptions

When deducing our three-state homo-FRET analytical model, which was used here to describe the coupled partition and oligomerization equilibria of Lz-A488 in interaction with anionic lipid membranes, several simplifying assumptions were made that must be discussed. First, a discrete oligomerization model,<sup>21</sup> rather than a nucleation-elongation model,<sup>44</sup> was used to describe lysozyme oligomerization in the lipid vesicles. This option stemmed from the need to reduce the number of free parameters involved in fitting the complex cooperative partition model combined with the Gouy-Chapman theory to the steady-state fluorescence anisotropy data of Lz-A488, which was already very large.<sup>21</sup> A more realistic description of the system would necessarily consider a distribution of oligomerization states, i.e. it should contemplate the formation of intermediate aggregates of variable sizes. This problem has already been addressed by Yeow and Clayton<sup>33</sup> who showed that the anisotropy plots for a distribution of oligomerization states presented a greater curvature than the discrete oligomerization model because in the distributed oligomer case states of higher oligomer number contribute to a stronger depolarization of the fluorescence. However, these differences were progressively more attenuated as the mean oligomerization number of the system under simulation increased from 1 to 4 (Fig. 2 from<sup>33</sup>). In fact, one expects that the homo-FRET terms obtained for a narrow distribution of oligomer sizes and for a discrete oligomerization model to become increasingly closer to each other upon increasing the mean oligomerization number of the system because the incremental decrease in overall anisotropy becomes smaller as the oligomer size increases.

Secondly, the possible contribution of a concentration depolarization effect (*i.e.* inter-monomeric or monomer-oligomer energy homo transfer) to the anisotropy experimental data was ignored. Assuming that both the membrane-bound monomers and oligomers are randomly distributed on the membrane surface, their average separation distance can be calculated using  $R_{av} = 1/2(\sqrt{\sigma})$ , where  $\sigma$  is the protein surface density.<sup>8</sup> For the experimental conditions described in Figs. 4 and S2, and assuming  $k = 6$  and  $K_{ag} = 2 \times 10^{14}$ ,  $R_{av}$  was always higher than 6.7 nm, which is much larger than our  $R_0$ . This rules

out the possibility that this effect might be significant even when a high surface coverage of the liposomes with Lz-A488 was attained.

Additionally, the theory proposed by Runnels and Scarlata to determine the number of subunits per oligomer was used herein.<sup>7</sup> Basically, this implies considering that the energy homo transfer process among the randomly oriented fluorescently-labeled proteins in a mixed oligomer is a very efficient process (interfluorophore distance  $R < 0.8 R_0$ ). In the absence of any rotational diffusion, this translates into the anisotropy of each oligomeric species,  $\langle r \rangle_{P_m^k}^i$ , being inversely proportional to the number  $i$  of labeled subunits in the oligomer because the anisotropy after one energy transfer step under these conditions is 0.016.<sup>45</sup> Noteworthy, this is a much less dramatic approximation than the one used by Yeow and Clayton in their work<sup>33</sup> since the authors admitted that the anisotropy of oligomers containing two or more fluorescently labeled subunits is zero. It can be easily deduced from eqn (13) that this is equivalent to (as used by the authors in their work to describe a bimodal monomer- $k$ -mer model):

$$\langle r \rangle_{P_m^k} = (1 - f)^{k-1} \cdot \langle r \rangle_{P_m^k}^{i=1} \quad (25)$$

As it is displayed in Fig. 2, the limits for the Yeow and Clayton's homo-FRET term are now  $\lim_{f \rightarrow 0}(\text{homo-FRET term})=1$  and  $\lim_{f \rightarrow 1}(\text{homo-FRET term})=0$ . It is also evident from this plot that this approximation largely overestimates the importance of homo-FRET within the oligomeric species assembled in a system.<sup>6</sup>

In the absence of any structural information regarding the quaternary structure adopted by the membrane-bound lysozyme molecules (relative orientation and packing of the monomers in each oligomer) that would allow us to build a geometric model for our clusters, it is difficult to accurately assess how strongly our system deviates from the assumptions underlying the theory of Runnels and Scarlata. Certainly, the molecules in an oligomer are expected to be partially aligned, and therefore the donor and acceptor transition dipoles are not totally uncorrelated. On the other hand, the steady-state anisotropy obtained here for the single-labeled membrane-bound lysozyme oligomer is much higher than the one retrieved for the monomeric species ( $\langle r \rangle_{P_m^k}^{i=1} = 0.35$  and  $\langle r \rangle_{P_m^1} = 0.25$ , respectively). This indicates that Lz-A488 is close to immobile within each oligomer during the excited-state lifetime of the probe, which is a favorable feature because the system is then closer to fulfill the requirement of rotationally fixed

fluorophores.<sup>7</sup> More importantly, it is expected that upon increasing the oligomer stoichiometry, some of the fluorophores become increasingly distant from each other within each oligomer. This implies that the condition that all interfluorophore distances are below the range for maximal FRET efficiency ( $R < 0.8 R_0$ ) must break down at some point, which critically depends on the particular 3D arrangement of the subunits within each oligomer, their individual dimensions and the modification site with the dye on the protein sequence. It should be noted, however, that in this case the anisotropy of each oligomeric species,  $\langle r \rangle_{\text{pk}}^i$ , would still be a function of the number  $i$  of labeled subunits in the oligomer, although no longer exactly proportional to  $1/k$ . In fact, energy transfer from a donor at a particular site to its nearest and second next-to-nearest neighbors must become dominant in this case due to the inverse dependence of the energy transfer rate with the sixth power of the distance between a pair of molecules. In the limit of very large clusters, the homo-FRET efficiency is expected to become independent of the oligomer size because then only the interactions established between the fluorescently-labeled molecules positioned closed to one another would be important.<sup>18</sup> This implies that our three-state homo-FRET model only allows estimating the minimal oligomerization stoichiometry of the membrane-bound proteins/peptides under study.

Finally, it should be emphasized that the cooperative partition model used here (Fig. 1) was able to successfully describe the interaction of Lz-A488 with phosphatidylserine-containing liposomes when two different fluorescence methodologies were employed to track the molar fraction of each fluorescent population in the system. In fact, the steady-state anisotropy (this study) and mean fluorescence lifetime (used earlier<sup>21</sup>) of the fluorescently-labeled protein reflect distinct photophysical properties of the fluorescently-labeled molecule. Although the steady-state anisotropy is related to the mean fluorescence lifetime of a fluorophore, we clearly show in this study that the progressive decrease in the mean fluorescence lifetime of Lz-A488 upon its oligomerization in the membrane cannot justify the concomitant changes occurring in its steady-state anisotropy. It should also be stressed that the propagation of the energy homo transfer occurring within the mixed oligomers to the overall anisotropy of each sample is mitigated in our system due to the lower quantum-yield of the oligomeric species. Additionally, both these studies illustrate the importance of exploring different experimental conditions in order to maximally populate each of the three fluorescent

species under study one at a time. This allows evaluating independently the anisotropy/mean fluorescence lifetime presented by the different monomeric and oligomeric states of Lz-A488, minimizing the problems associated with the high correlation between several of the parameters used to describe this complex three-state model. Also, the results obtained become much more reliable since the ability to discriminate among models of different quaternary stoichiometry is tested under a much wider set of conditions.

## Conclusions

In the present work, we derived a general quantitative method for deducing the oligomer stoichiometry of membrane-bound proteins involved in a three-state cooperative partition equilibrium by energy homo transfer measurements. This relies on the use of a simple analytical equation describing the relationship between the oligomer steady-state fluorescence anisotropy and intra-oligomeric fluorescence homotransfer as a function of the fractional labeling of the sample when the limit of Runnels and Scarlata is valid (i.e. when the fluorescence anisotropy is inversely related to the oligomer stoichiometry at short transfer distances,  $R < 0.8 R_0$ ).<sup>7</sup> This equation is more general than the one proposed earlier by Yeow and Clayton<sup>33</sup> because it no longer assumes that the anisotropy of mixed oligomers containing more than one fluorophore is zero. This method was tested in a steady-state fluorescence anisotropy based homo-FRET study of fluorescently-labeled lysozyme in interaction with anionic lipid membranes. Time-resolved anisotropy decays confirmed that energy homo transfer was the source of the observed fluorescence depolarization at high surface coverage of the liposomes by Lz-A488. This model was globally fitted to the steady-state anisotropies obtained for Lz-A488 in seven independent experiments that explored a broad range of experimental conditions (variable total protein and lipid concentrations, protein labeling ratios and anionic lipid content of the liposomes), allowing to narrow down the membrane-bound oligomer stoichiometry of Lz-A488 to a minimum of  $k = 6 \pm 1$ . This study illustrates the effectiveness of using homo-FRET measurements to monitor the oligomerization state of membrane-bound peptides/proteins even in the presence of an additional monomer membrane/water partition equilibrium.

## Acknowledgments

We thank Professor Mário Nuno Berberan-Santos for useful scientific discussions. A.M. acknowledges the support of Fundação para a Ciência e Tecnologia (FCT) via SFRH/BD/61723/2009. This work was supported by projects PTDC/QUI-BIQ/099947/2008, PTDC/BBB-BQB/2661/2012 and RECI/CTM-POL/0342/2012 from FCT.

## References

1. T. Pawson and P. Nash, *Genes Dev.*, 2000, **14**, 1027-1047.
2. F. K. M. Chan, *Cytokine*, 2007, **37**, 101-107.
3. J. A. Hebda and A. D. Miranker, *Ann. Rev. Biophys.*, 2009, **38**, 125-152.
4. S. M. Butterfield and H. A. Lashuel, *Angew. Chem.-Int. Edit.*, 2010, **49**, 5628-5654.
5. A. N. Bader, S. Hoetzel, E. G. Hofman, J. Voortman, P. M. van Bergen en Henegouwen, G. van Meer and H. C. Gerritsen, *Chemphyschem*, 2011, **12**, 475-483.
6. F. T. Chan, C. F. Kaminski and G. S. Kaminski Schierle, *Chemphyschem*, 2011, **12**, 500-509.
7. L. W. Runnels and S. F. Scarlata, *Biophys. J.*, 1995, **69**, 1569-1583.
8. B. Valeur and M. N. Berberan-Santos, *Molecular Fluorescence. Principles and Applications*, Wiley-VCH, Weinheim, 2012.
9. S. M. Blackman, D. W. Piston and A. H. Beth, *Biophys. J.*, 1998, **75**, 1117-1130.
10. M. P. Lillo, O. Canadas, R. E. Dale and A. U. Acuna, *Biochemistry*, 2002, **41**, 12436-12449.
11. H. Otto, T. Lamparter, B. Borucki, J. Hughes and M. P. Heyn, *Biochemistry*, 2003, **42**, 5885-5895.
12. S. L. Robia, N. C. Flohr and D. D. Thomas, *Biochemistry*, 2005, **44**, 4302-4311.
13. T. J. van Ham, A. Esposito, J. R. Kumita, S. T. Hsu, G. S. Kaminski Schierle, C. F. Kaminski, C. M. Dobson, E. A. Nollen and C. W. Bertocini, *J. Mol. Biol.*, 2010, **395**, 627-642.
14. P. Sharma, R. Varma, R. C. Sarasij, Ira, K. Gousset, G. Krishnamoorthy, M. Rao and S. Mayor, *Cell*, 2004, **116**, 577-589.
15. A. N. Bader, E. G. Hofman, J. Voortman, P. M. P. van Bergen en Henegouwen and H. C. Gerritsen, *Biophys. J.*, 2009, **97**, 2613-2622.
16. E. G. Hofman, A. N. Bader, J. Voortman, D. J. van den Heuvel, S. Sigismund, A. J. Verkleij, H. C. Gerritsen and P. Henegouwen, *J. Biol. Chem.*, 2010, **285**, 39481-39489.

17. S. Ganguly, A. H. A. Clayton and A. Chattopadhyay, *Biophys. J.*, 2011, **100**, 361-368.
18. H. D. Vishwasrao, P. Trifilieff and E. R. Kandel, *Biophys. J.*, 2012, **102**, 1204-1214.
19. W. C. Wimley, K. Hristova, A. S. Ladokhin, L. Silvestro, P. H. Axelsen and S. H. White, *J. Mol. Biol.*, 1998, **277**, 1091-1110.
20. A. Coutinho and M. Prieto, *Biophys. J.*, 2003, **84**, 3061-3078.
21. A. M. Melo, J. C. Ricardo, A. Fedorov, M. Prieto and A. Coutinho, *J. Phys. Chem. B*, 2013, **117**, 2906-2917.
22. A. M. Melo, L. M. S. Loura, F. Fernandes, J. Villalain, M. Prieto and A. Coutinho, *Soft Matter*, 2014, **10**, 840-850.
23. A. M. Melo, M. Prieto and A. Coutinho, *Biochim. Biophys. Acta-Biomembr.*, 2011, **1808**, 2559-2568.
24. R. P. Haugland, ed. *The Handbook. A Guide to Fluorescent Probes and Labeling Technologies (10th ed.)*, Molecular Probes, Eugene, OR2005.
25. C. N. Pace, F. Vajdos, L. Fee, G. Grimsley and T. Gray, *Protein Sci.*, 1995, **4**, 2411-2423.
26. C. W. F. McClare, *Anal. Biochem.*, 1971, **39**, 527-530.
27. Lakowicz, ed. *Principles of fluorescence spectroscopy*, Springer, New York, 2006.
28. B. R. Lentz, B. M. Moore and D. A. Barrow, *Biophys. J.*, 1979, **25**, 489-494.
29. J. A. Poveda, M. Prieto, J. A. Encinar, J. M. Gonzalez-Ros and C. R. Mateo, *Biochemistry*, 2003, **42**, 7124-7132.
30. R. F. de Almeida, L. M. Loura, M. Prieto, A. Watts, A. Fedorov and F. J. Barrantes, *Mol. Membr. Biol.*, 2006, **23**, 305-315.
31. M. N. Berberan-Santos and M. J. E. Prieto, *J. Chem. Soc., Faraday Trans. 2*, 1987, **83**, 1391-1410.
32. G. Weber and F. W. J. Teale, *Trans. Faraday Soc.*, 1957, **53**, 646-655.
33. E. K. L. Yeow and A. H. A. Clayton, *Biophys. J.*, 2007, **92**, 3098-3104.
34. D. Suckau, M. Mak and M. Przybylski, *Proc. Natl. Acad. Sci. U.S.A.*, 1992, **89**, 5630-5634.
35. G. P. Gorbenko, V. M. Ioffe and P. K. J. Kinnunen, *Biophys. J.*, 2007, **93**, 140-153.
36. G. Lipari and A. Szabo, *Biophys. J.*, 1980, **30**, 489-506.
37. I. Pastor, M. L. Ferrer, M. P. Lillo, J. Gomez and C. R. Mateo, *J. Phys. Chem. B*, 2007, **111**, 11603-11610.
38. K. Kinosita, S. Kawato and A. Ikegami, *Biophys. J.*, 1977, **20**, 289-305.
39. G. F. Schroder, U. Alexiev and H. Grubmuller, *Biophys. J.*, 2005, **89**, 3757-3770.

40. E. Rusinova, V. Tretyachenko-Ladokhina, O. E. Vele, D. F. Seneor and J. B. A. Ross, *Anal. Biochem.*, 2002, **308**, 18-25.
41. J. Karolin, L. B. A. Johansson, L. Strandberg and T. Ny, *J. Am. Chem. Soc.*, 1994, **116**, 7801-7806.
42. C. C. F. Blake, D. F. Koenig, G. A. Mair, A. C. T. North, D. C. Phillips and V. R. Sarma, *Nature*, 1965, **206**, 757-761.
43. F. Tanaka and N. Mataga, *Photochem. Photobiol.*, 1979, **29**, 1091-1097.
44. G. Klocek, T. Schulthess, Y. Shai and J. Seelig, *Biochemistry*, 2009, **48**, 2586-2596.
45. M. N. Berberan-Santos and B. Valeur, *J. Chem. Phys.*, 1991, **95**, 8048-8055.

## Figure legends

**Figure 1 – Probing the membrane-bound oligomer stoichiometry of fluorescently-labeled proteins/peptides involved in a cooperative partition equilibrium using homo-FRET measurements.** (a) Schematic representation of the three-state model used to describe the interaction of proteins/peptides with anionic lipid membranes: monomeric proteins/peptides partition to the bilayer surface and reversibly assemble into  $k$ -mers (here exemplified for a tetrameric species). (b) Absorption and fluorescence emission spectra of 1.5  $\mu\text{M}$  Lz-A488 ( $DoL = f = 0.21$ ) in 20 mM HEPES-KOH, 0.1 mM EDTA, pH 7.4 buffer. Due to its small Stokes shift, Lz-A488 has a high potential for homo-FRET. (c) Only the fluorescent species of the system contribute to the overall anisotropy of the sample. The binomial distribution of fluorescently-labeled monomers per oligomer must be taken into account to describe the homo-FRET contribution from each mixed oligomeric species. In the limit of very efficient energy homo transfer, the steady-state anisotropy of oligomers with  $i$ -labeled monomers is inversely proportional to the number of labeled subunits per oligomer (eqn (14)). See the text for more details.

**Figure 2 – Variation of the homo-FRET term (i.e. the ratio  $\langle r \rangle_{P_m^k} / \langle r \rangle_{P_m^{i=1}}$ ) for different  $k$ -mers with the fluorescent labeling ratio,  $f$ , of the sample.** The solid lines reflect the contribution of all fluorescently-labeled oligomers ( $i \geq 1$ ) to the fluorescence depolarization of the sample (eqn (15)), whereas the dashed lines represent the situation when the anisotropy of the oligomers containing two or more fluorescently labeled monomers is considered to be zero (eqn (25)):  $k=2$  (dark blue lines),  $k=4$  (cyan lines),  $k=6$  (green lines) and  $k=8$  (red lines), respectively.

**Figure 3 – Fluorescence anisotropy decays from free and membrane-bound monomeric Lz-A488.** The blue and red solid lines are the best fitting curves of eqn (6) to the anisotropy decays obtained for Lz-A488 in buffer (1.5  $\mu\text{M}$ ,  $DoL = f = 0.21$ ) and in the presence of 4 mM POPC:POPS 80:20 LUVs (0.5  $\mu\text{M}$ ,  $DoL = f = 0.21$ ), respectively (see Table 1). The residuals of each fit are also shown.

**Figure 4 – The extent of homo-FRET critically depends on the membrane surface density of Lz-A488.** Changes in the steady-state anisotropy of Lz-A488 as a function of (a, b) total phospholipid, (c) protein concentration and (d) fractional labeling of the sample. The specific conditions used were: (a) 0.5  $\mu\text{M}$  lysozyme,  $DoL = f = 0.54$ ; (b) 3.0  $\mu\text{M}$  lysozyme,  $DoL = f = 0.30$  ( $\circ$ ) and 0.54 ( $\bullet$ ); (c) variable lysozyme concentration,  $DoL = f = 0.54$ ; (d) 6  $\mu\text{M}$  lysozyme, variable  $f$ ; (c and d) 0.86 mM total phospholipid concentration. The lipid composition of the liposomes was POPC:POPS 80:20. The blue solid curves are the best-fit of eqn (17) to the steady-state anisotropy data ( $k = 6$  and  $K_{ag} = 2 \times 10^{14}$ ). The cyan, green and red (and magenta in panel (b)) dotted dashed lines represent the contribution of each individual species (aqueous and membrane-bound monomeric and oligomeric species, respectively) to the overall anisotropy of the sample. In panel (b), red and magenta dotted dashed lines correspond to  $DoL = f = 0.54$  and 0.30, respectively. In panel (d), the cyan and green dotted dashed lines are super-imposed.

**Figure 5 –Homo-FRET within the mixed membrane-bound lysozyme oligomers strongly affects the fluorescence anisotropy decays of Lz-A488 in interaction with 0.86 mM POPC:POPS 80:20 LUVs.** The solid lines are the best fitting curves of eqn (6) to the anisotropy decays obtained for (a) 0.3 and 6  $\mu\text{M}$  lysozyme ( $DoL = f = 0.54$ ) (red and blue lines, respectively) and (b) 6  $\mu\text{M}$  lysozyme prepared with variable fractional labeling (blue, red and green lines for  $f = 0.34$ ,  $f = 0.11$  and  $f = 0.03$ , respectively) (see Table 1). The residuals of each fit are also shown.

**Figure 6 –** (a) Dependency of the minimum mean-square deviation (MSD) with the oligomer stoichiometry,  $k$ , obtained from fitting the three-state homo-FRET model (eqn (17)) to the experimental data of Fig. 4 and S2. Compared to the results obtained in a previous study (inset),<sup>21</sup> the oligomerization state of lysozyme was now narrowed down to  $k = 6 \pm 1$ .

Figure 1

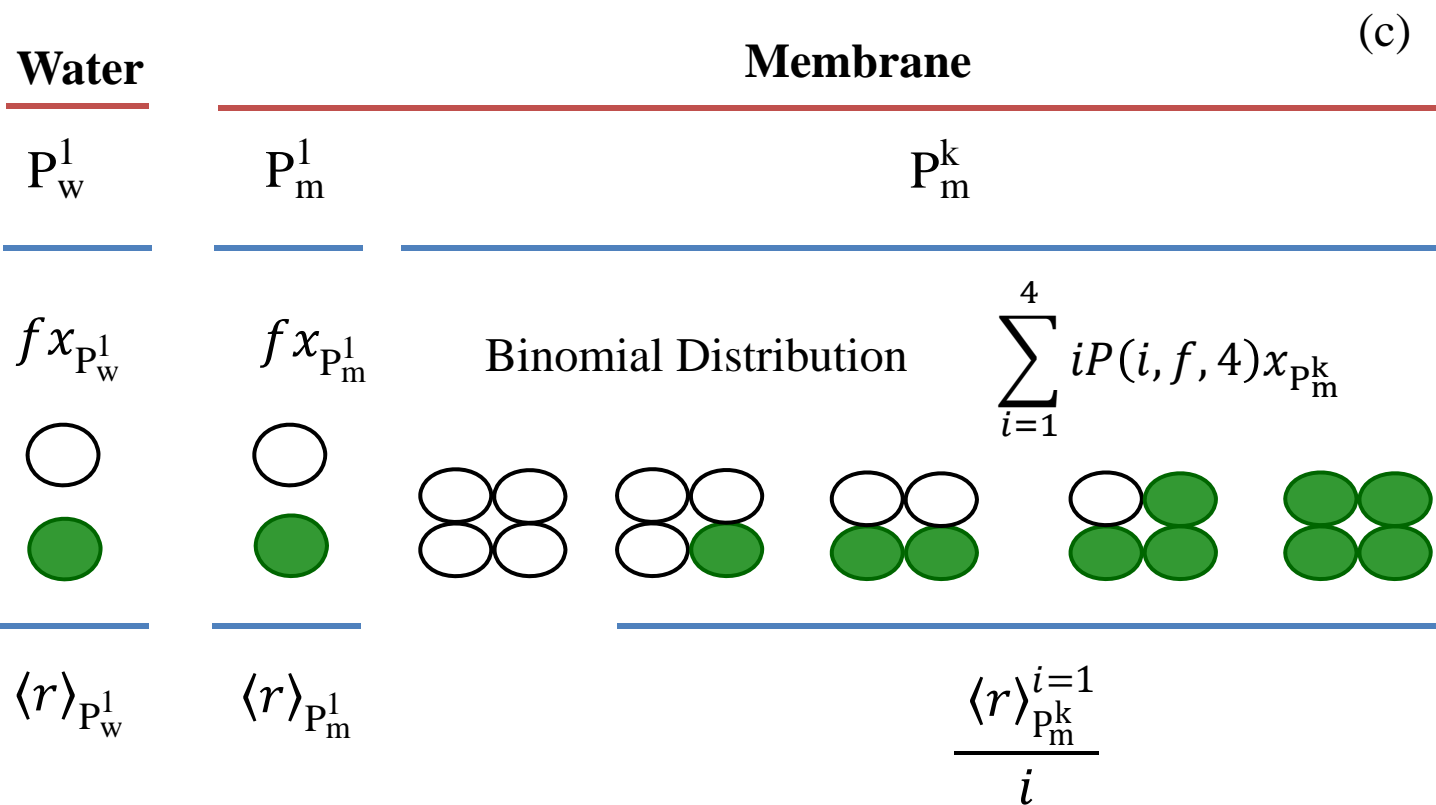
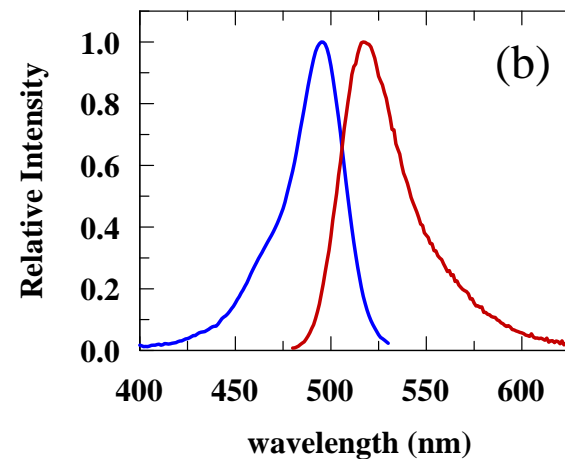
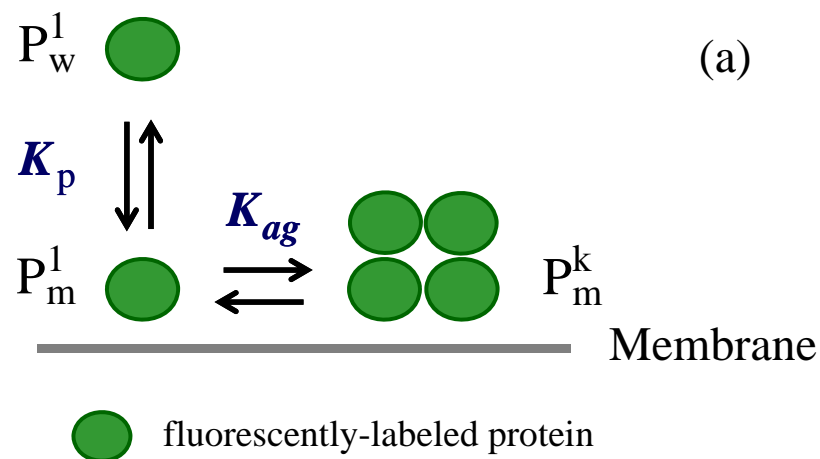


Figure 2

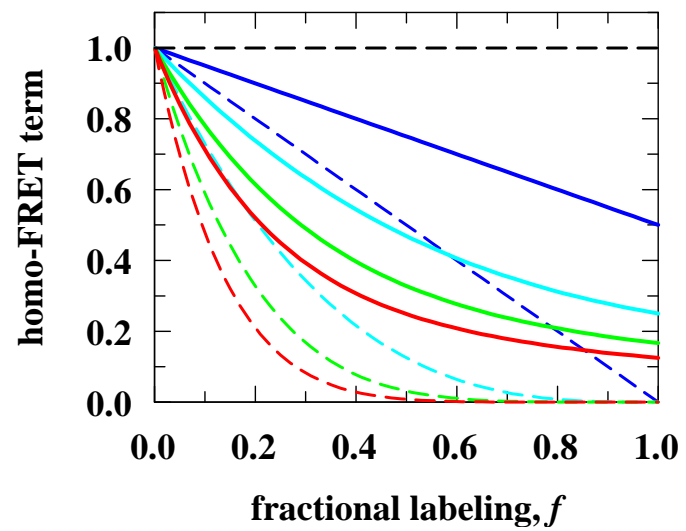


Figure 3

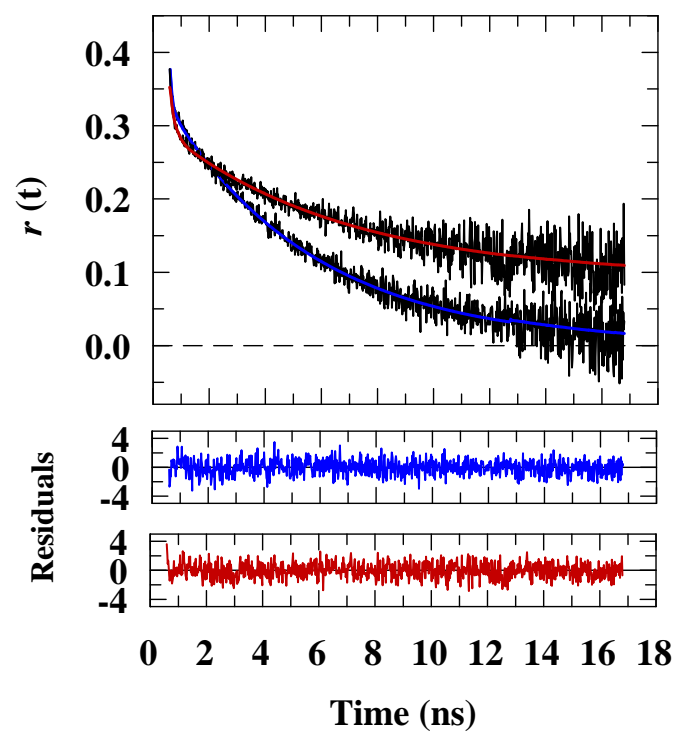


Figure 4

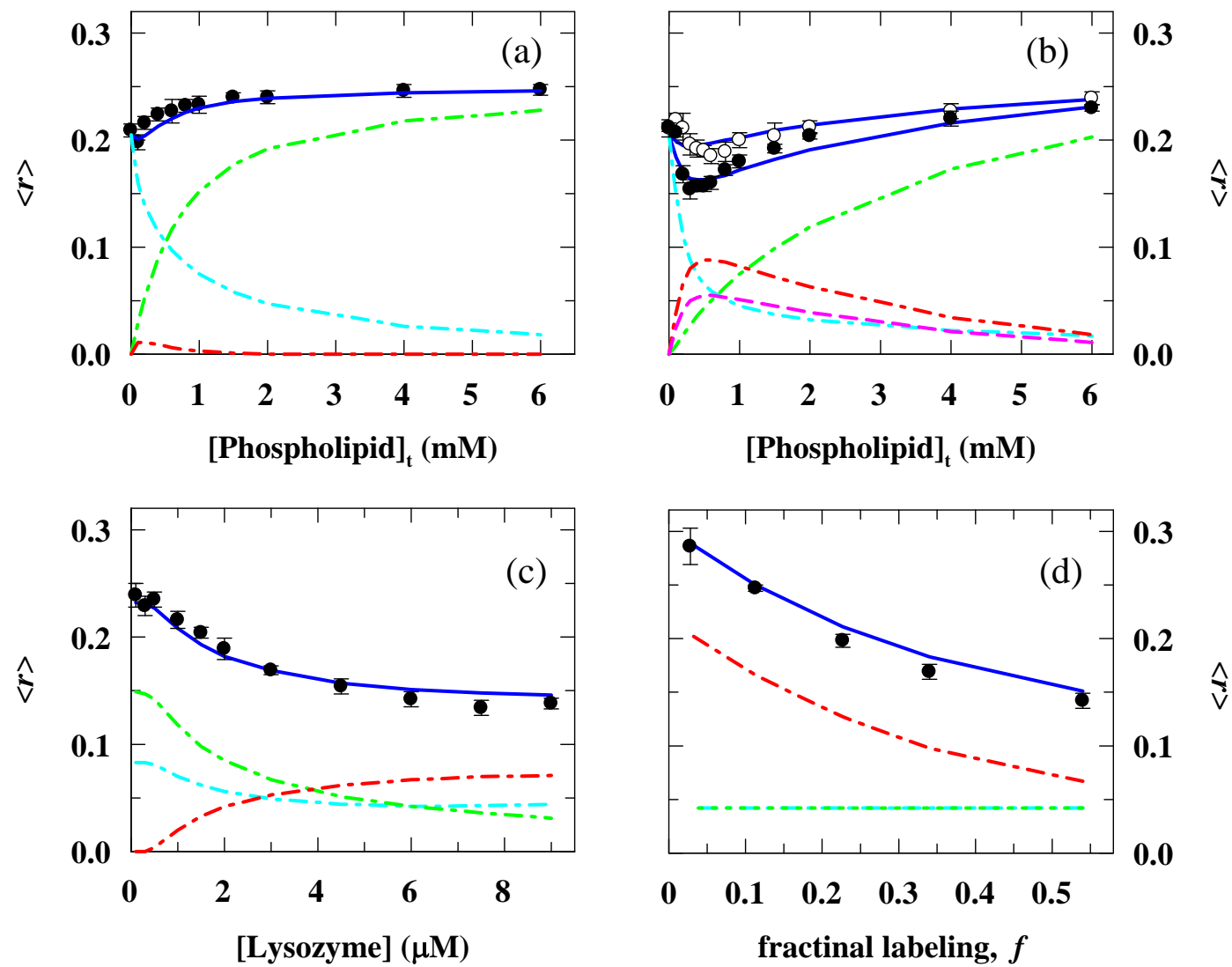


Figure 5

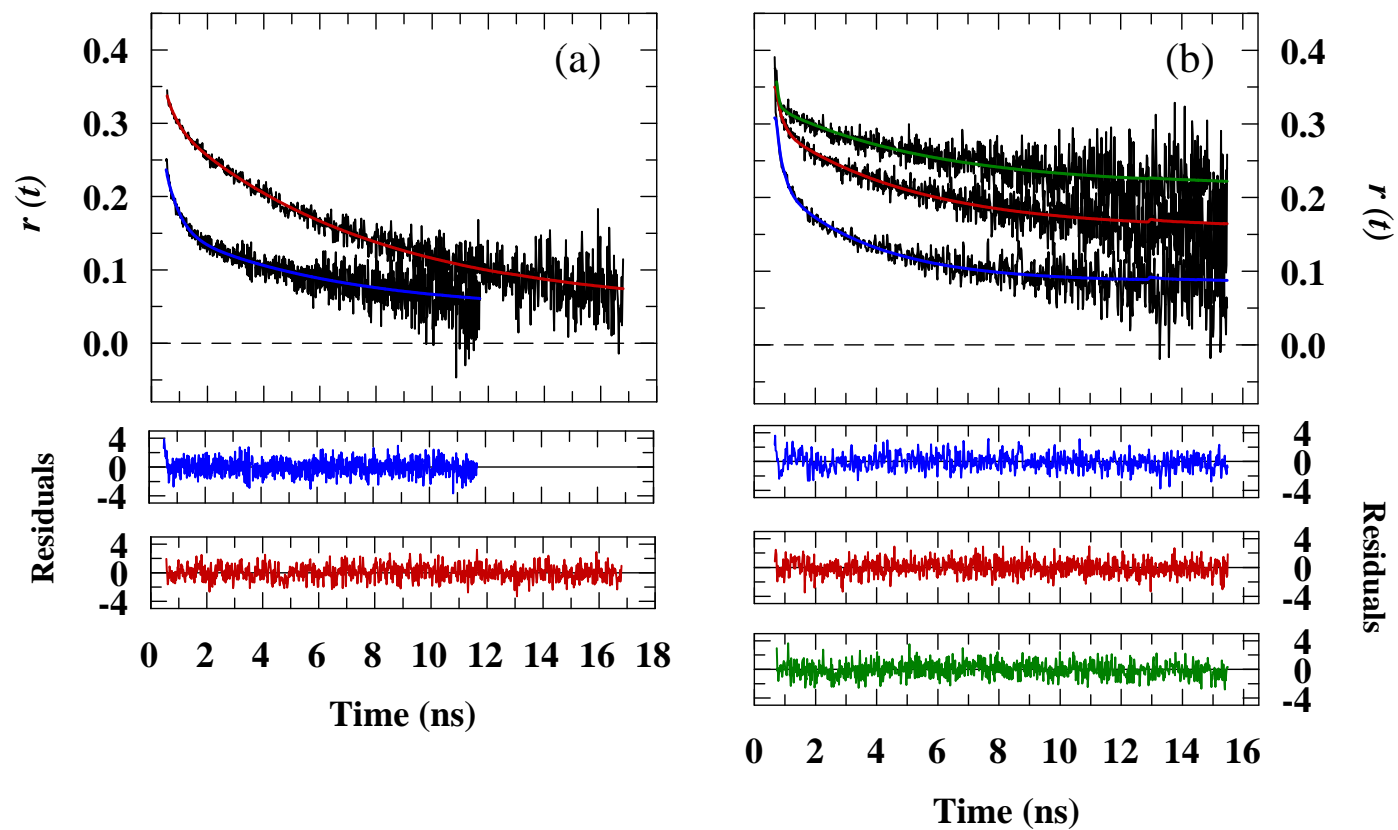


Figure 6

